# Quantum phase transition in the *XXZ* central spin model

Lei Shao [1,2] Rui Zhang,[2] Wangjun Lu [3] Zhucheng Zhang,[2] and Xiaoguang Wang[1,2,*]

[1]*Key Laboratory of Optical Field Manipulation of Zhejiang Province and Department of Physics, Zhejiang Sci-Tech University, Hangzhou 310018, China*

[2]*Zhejiang Institute of Modern Physics, Department of Physics, Zhejiang University, Hangzhou 310027, China*

[3]*Department of Maths and Physics, Hunan Institute of Engineering, Xiangtan 411104, China*

We investigate the quantum phase transition (QPT) in the *XXZ* central spin model, which can be described as a spin-$\frac{1}{2}$ particle coupled to $N$ bath spins. In general, the QPT is supposed to occur only in the thermodynamical limit. In contrast, we present that the central spin model exhibits a normal-to-superradiant phase transition in the limit where the ratio of the transition frequency of the central spin to that of the bath spins and the number of bath spins tend to infinity. We give the low-energy effective Hamiltonian analytically in the normal phase and the superradiant phase, and we find that the longitudinal interaction $\Delta$ can significantly influence the excitation number and the coherence of the ground state. These two quantities are remarkably enhanced for the negative longitudinal interaction while suppressed for the positive longitudinal interaction. In addition, the finite-size effect on the central spin model is also illustrated through the mean-field analysis. We further exploit the quantum Fisher information to characterize the QPT and propose a measurement scheme that can be applied in practice. This work builds a connection between the qubit-spin systems and the qubit-field systems, which provides a possibility for the realization of criticality-enhanced quantum sensing in central spin systems.

## I. INTRODUCTION

Quantum phase transition (QPT) of many-body systems plays an important role in our understanding of physics [1]. While Landau's symmetry-breaking theory gains great success in describing thermal phase transitions, quantum phase transitions, which are due to quantum fluctuations when the temperature goes to zero beyond the symmetry-breaking paradigm, attract a lot of interest in condensed matter physics [2–9] and quantum optics [10–18]. As a well-known model in quantum optics, the Dicke model [10] describes $N$ two-level atoms coupled to a single-mode cavity, and a quantum phase transition from the normal phase to the superradiant phase will occur in the thermodynamic limit of $N \rightarrow \infty$. Recently, Hwang *et al.* [19,20] presented that QPT can occur under the situation of a two-level atom coupled to a single-mode cavity, and they indicated that the ratio $\eta$ of the atomic transition frequency to the cavity field frequency plays the same role in the quantum Rabi model (QRM) and the Jaynes-Cummings model (JC) as the number of atoms in the Dicke model and the Tavis-Cummings model [21]. They also showed that the two-site JC lattice undergoes a Mott-insulator–superfluid QPT in the limit of $\eta \rightarrow \infty$ [20].

Actually, there exists a similarity between the light-matter interaction in optical systems and the hyperfine interaction in spin systems. Like the phenomenon of superradiance in quantum optics mentioned earlier, the superradiant effect can occur in the nuclear spin environment [22–26]. Kessler *et al.* [22] showed that the superradiant effect can be realized in

systems with a nuclear spin ensemble surrounding a quantum dot or a nitrogen-vacancy (NV) center, and some suitable optical pumping conditions used for implementation are given. In Ref. [27], Dooley *et al.* exploited the spin coherent state as the initial state to discuss the collapse and revival phenomena in the qubit–big spin model and revealed the similarities of the Hamiltonian between the qubit-spin systems and the qubit-field systems. In Ref. [28], He *et al.* gave the exact quantum dynamics of the *XXZ* central spin model, and the analytic expression of quantum collapse and revival was also obtained. Moreover, they used the Holstein-Primakoff transformation to build a mapping between the central spin model and the JC model. Furthermore, the connection between the spin-$s$ central spin model and the Tavis-Cummings model is discussed in Ref. [29].

However, the superradiant QPT has not been widely discussed in anisotropic central spin systems. Inspired by the work mentioned above, we follow the thoughts in Refs. [19,20,28] and analytically analyze the superradiant quantum phase transition in the *XXZ* central spin model. We first give the exact energy spectrum of the *XXZ* central spin model, and the asymptotic behavior between the central spin model and the JC model can be clearly observed in the case of a large number of the bath spins. The strength of longitudinal interaction $\Delta$ in the *XXZ* central spin model is different from that of the transverse interaction $A$, which can significantly influence the critical point of the phase transition. Thus, it is necessary to discuss the two following cases: (i) $\Delta = 0$ and (ii) $|\Delta| < \omega$, where $\omega$ is the frequency of the bath spins. It shows that the *XXZ* central spin model has a similar critical point to the JC model under the condition of $\Delta = 0$. However, for $|\Delta| < \omega$, the critical point is different from the one before,

*xgwang@zstu.edu.cn

and we give an analytical solution for this by means of the theory of low-energy effective Hamiltonian.

This article is organized as follows. In Sec. II, we give the exact energy spectrum of the *XXZ* central spin model and obtain the analytic expression of excitation number via the mean-field approximation. In Sec. III, we present the derivation of the low-energy effective Hamiltonian and exploit it to analyze the critical point and the ground state energy. In Sec. IV, we discuss the influence of the longitudinal interaction $\Delta$ on the excitation number and the coherence of the ground state. In Sec. V, we investigate the finite-size effect in the central spin model. In Sec. VI, we make use of the quantum Fisher information (QFI) to characterize the QPT of the *XXZ* central spin model, and give a measurement scheme. Finally, we give a conclusion in Sec. VII.

## II. MODEL

The central spin model can be described as a single spin-$\frac{1}{2}$ particle coupled to $N$ spin-$\frac{1}{2}$ particles (bath spins), which is also called the qubit–big spin model in Ref. [27]. For different strengths of the longitudinal and the transverse interactions, the Hamiltonian of this model can be written as [28] (we set $\hbar = 1$)

$$H = \frac{\omega_0}{2}\sigma_z^{(0)} + \frac{\omega}{2}\sum_{k=1}^{N}\sigma_z^{(k)} + \sum_{k=1}^{N}\frac{\Delta_k}{2}\sigma_z^{(k)}\sigma_z^{(0)}$$
$$+ \sum_{k=1}^{N}\frac{A_k}{2}\left(\sigma_x^{(k)}\sigma_x^{(0)} + \sigma_y^{(k)}\sigma_y^{(0)}\right), \quad (1)$$

where $\omega_0$ and $\omega$ are, respectively, the transition frequency of the central spin and bath spins, $A_k$ is the strength of transverse interaction, and $\Delta_k$ is the longitudinal interaction. $\sigma_i^0$ denotes the Pauli operator of the central spin and $\sigma_i^{(k)}$ ($i = x, y, z$) denotes the Pauli operator of the bath spins. The central spin model is widely applied to solve the problem in quantum dots [30–33] and nitrogen-vacancy (NV) centers [34], and the bath spins can be regarded as a big spin or a quantum reference frame [35–37], which can be promising in quantum metrology [38–44]. For simplicity, we consider the case that the central spin is uniformly coupled to bath spins ($A_k = A$, $\Delta_k = \Delta$), and the Hamiltonian becomes

$$H = \omega_0 S_z + \omega J_z + A(J_+ S_- + J_- S_+) + 2\Delta J_z S_z, \quad (2)$$

where $S_z = \frac{1}{2}\sigma_z^{(0)}$, $J_z = \frac{1}{2}\sum_{k=1}^{N}\sigma_z^{(k)}$, and $N$ bath spins can be equivalent to a big spin with spin $j$ ($j = N/2$). From Eq. (2), we see that the Hamiltonian of the *XXZ* central spin model exhibits a $U(1)$ symmetry. Now we introduce the Dicke states $|N/2, m\rangle = |j, m\rangle$ ($m \in [-j, j]$) as the eigenstates of $J_z$ and $|\uparrow\rangle$ ($|\downarrow\rangle$) as the eigenstate of $\sigma_z^{(0)}$.

In this paper, we denote $|\uparrow(\downarrow)\rangle \otimes |j, n-j\rangle$ as $|\uparrow(\downarrow), n\rangle$ ($n \in [0, 2j]$), and $n$ can be viewed as the excitation number of bath spins. Note that the states $|\uparrow, n-1\rangle$ and $|\downarrow, n\rangle$ are analogous to the bare states [45] of the JC model. Due to the $U(1)$ symmetry of the Hamiltonian in Eq. (2), it is easy to obtain the energy eigenvalues

$$E_{\pm,n} = \frac{1}{2}\Big[(2m+1)\omega - \Delta$$
$$\pm\sqrt{[(2m+1)\Delta - \omega + \omega_0]^2 + 4A^2 k_n}\Big], \quad (3)$$

where $m = n - 1 - j$, $k_n = 2j - n + 1$. More detailed derivations are presented in Appendix A.

Up to now we have not discussed the value range of the parameter $\Delta$. Note that $|\downarrow, 0\rangle$ is the ground state of Eq. (2) for $|\Delta| < \omega$, and its eigenvalue is $E_{\downarrow,0} = -\frac{\omega_0}{2} - (\omega - \Delta)j$. In the subsequent sections, we will prove $\omega < |\Delta|$ is a necessary condition for the superradiance QPT in the *XXZ* central spin model, and we will also discuss the influence of different $\Delta$ on the *XXZ* central spin model. Now we introduce

$$\eta = \frac{\omega_0}{\omega}, \quad g = \frac{A\sqrt{2j}}{\sqrt{\omega_0\omega}} = \frac{\lambda}{\sqrt{\omega_0\omega}}, \quad (4)$$

which are the frequency ratio and the dimensionless coupling strength, respectively. In order to make $g$ satisfy $g \sim O(1)$ in the limit of $\eta \to \infty$, we need to ensure that $\lambda/\omega \sim \sqrt{\eta}$. For $\Delta = 0$ and $\eta \gg 1$, $E_{-,n}$ in Eq. (3) can be expanded to

$$E_{-,n} = -\frac{\omega_0}{2} - \omega j + \left(1 - g^2 + g^2\frac{n-1}{2j}\right)n\omega + O(\eta^{-1}). \quad (5)$$

In the $N \to \infty$ limit, the nonlinear term in Eq. (5) can be negligible and we obtain $E_{-,n} = (1 - g^2)n\omega + E_{\downarrow,0}$, which has a similar harmonic spectrum presented in Ref. [20]. For $g < 1$, $E_{-,n}$ is minimum at $n = 0$ and the ground state energy in the normal phase is $-\omega_0/2 - \omega j$. For $g = 1$, there exists a degeneracy between $|\psi_-(n)\rangle$ [Eq. (A4)] and $|\downarrow, 0\rangle$ and the normal-to-superradiant phase transition occurs at this critical point. It is clear to see that for $g > 1$ the ground state is instable and its energy can decrease infinitely as the excitation number increases, and the bath spins are macroscopically excited just like the behavior of the cavity field in the JC model [20].

Now we calculate the excitation number of the ground state. For $N \gg n$ and $\eta \gg 1$, $E_{-,n}$ in Eq. (3) can be written as

$$E_{-,n} = -\frac{\omega_0}{2}\sqrt{1 + 4g^2 n\eta^{-1}} + \omega_0(n - j - 1)\eta^{-1}, \quad (6)$$

and utilizing $(\partial E_{-,n}/\partial n)/\omega_0 = 0$, we find that the excitation number of the ground state is $n_g = 0$ for $g < 1$. For $g > 1$, the excitation number becomes

$$n_g = \frac{\eta}{4}(g^2 - g^{-2}), \quad (7)$$

which is consistent with the result in Ref. [20].

It is hard to acquire an analytical expression of excitation number $n_g$ for $|\Delta| < \omega$ from Eq. (3), thus we use the mean-field approximation to get the mean-field energy, which is given by

$$E^{\mathrm{MF}}(n) = \omega(n - j) - \frac{1}{2}\overline{\omega}_0(n), \quad (8)$$

where $\overline{\omega}_0(n) = \sqrt{4\lambda^2 n + 4n^2\Delta^2 + 4n\Delta\widetilde{\omega}_0 + \widetilde{\omega}_0^2}$, and $\widetilde{\omega}_0 = \omega_0 - N\Delta$.

In the normal phase, the excitation number of the ground state is still $n_g = 0$. But for the superradiant phase, the excitation number is given by

$$n_g = -\frac{\lambda^2 + \Delta\widetilde{\omega}_0}{2\Delta^2} + \frac{\lambda\omega}{2\Delta^2}\sqrt{\frac{\lambda^2 + 2\Delta\widetilde{\omega}_0}{\omega^2 - \Delta^2}}, \quad (9)$$

and the ground state energy under the mean-field approximation is given by

$$E_g^{\mathrm{MF}} = \omega(n_g - j) - \tfrac{1}{2}\overline{\omega}_0(n_g), \tag{10}$$

where

$$\overline{\omega}_0(n_g) = \tilde{g}\widetilde{\omega}_0\sqrt{\frac{\tilde{g}^2\widetilde{\omega} + 2\Delta}{\widetilde{\omega} + 2\Delta}}, \tag{11}$$

and $\tilde{g} = \lambda/\sqrt{\widetilde{\omega}\widetilde{\omega}_0}$, $\widetilde{\omega} = \omega - \Delta$. The detailed derivation is presented in Appendix A. This result is completely different from the previous situation due to the existence of the nonlinear coupling term [46].

## III. LOW-ENERGY EFFECTIVE HAMILTONIAN

In order to further understand the QPT in the *XXZ* central spin model, in this section we give the low-energy effective Hamiltonian in both the normal phase and the superradiant phase. Note that Eq. (2) can be mapped to the Hamiltonian of the JC model when $\Delta = 0$, which has been discussed in detail in Ref. [20], thus we focus on $|\Delta| < \omega$ in this paper.

For the normal phase, we apply a Holstein-Primakoff transformation and a Schrieffer-Wolff transformation $e^S$ with the anti-Hermitian operator $S = \lambda(a^\dagger S_- - a S_+)/\widetilde{\omega}_0$ [19,20] to Eq. (2), and we obtain the low-energy effective Hamiltonian, which is

$$\widetilde{H}_{\mathrm{np}} = -\frac{\widetilde{\omega}_0}{2} - \omega j + \widetilde{\omega}(1 - \tilde{g}^2)a^\dagger a, \tag{12}$$

where $a$ ($a^\dagger$) is the bosonic annihilation (creation) operator. The detailed derivation of $\widetilde{H}_{\mathrm{np}}$ is presented in Appendix B. Equation (12) shows a similar structure to Eq. (5) in the $N \to \infty$ limit.

Now we prove that $|\Delta| < \omega$ is a necessary condition to acquire the QPT similar to the JC model. First of all, the comparison between Eq. (5) and Eq. (12) shows that $\widetilde{\omega}$ should satisfy that $\widetilde{\omega} > 0$, thus we have $\Delta < \omega$. Secondly, $n_g$ in Eq. (9) only makes sense if

$$\frac{\lambda^2 + 2\Delta\widetilde{\omega}_0}{\omega^2 - \Delta^2} > 0, \tag{13}$$

and it is easy to verify that Eq. (13) can always be satisfied if $\Delta > -\omega$ in the range of $\tilde{g} > 1$. Finally, we get the necessary condition for the superradiance QPT in the *XXZ* central spin model as $|\Delta| < \omega$.

From Eq. (12) we see that the new critical point for $|\Delta| < \omega$ is $\tilde{g}_c = \lambda/\sqrt{\widetilde{\omega}_0\widetilde{\omega}} = 1$. For $\tilde{g} < 1$, the ground state is $|\psi_g^{\mathrm{np}}\rangle = |\downarrow, 0\rangle$ with energy $E_{\mathrm{np}} = -\widetilde{\omega}_0/2 - \omega j$. Note that if $\Delta < \omega$ is not satisfied, then the ground state is $|\uparrow, 0\rangle$, which is not what we expect. However, the *XXZ* central spin model exhibits instability when $\tilde{g} > 1$, and to solve this problem, we use the method proposed in Refs. [19,20] to get the low-energy effective Hamiltonian in the superradiant phase.

Unlike the previous approach, we need to apply a displacement operator in addition to the two transformations mentioned before. Finally, we obtain the low-energy effective Hamiltonian as

$$\overline{H}'_{\mathrm{sp}} = \omega\alpha^2 - \frac{\overline{\omega}_0(n_g)}{2} + \kappa_0 x^2 - \omega j, \tag{14}$$



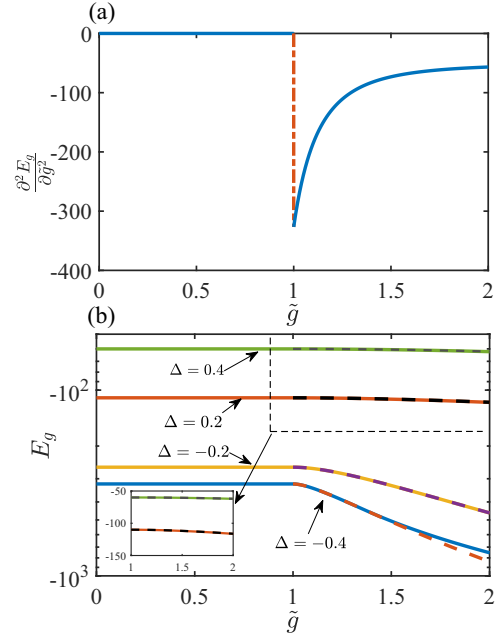FIG. 1. (a) Second derivative of the ground state energy with respect to $\tilde{g}$ in the limit of $\eta \to \infty$ and $N \to \infty$. (b) Ground state energy of the *XXZ* central spin model for different longitudinal interactions $\Delta$. Here we set $\omega_0 = 100$, $\omega = 0.5$. The solid lines are the result of the numerical simulation and the dashed lines are that of the analytical expression in Eq. (10). The top two curves (dark gray line and black line) fit better than the bottom two (purple line and red line).

where

$$\kappa_0 = \frac{\omega}{4} - \frac{2|\alpha|^2\Delta^2 + \Delta\widetilde{\omega}_0}{4\overline{\omega}_0} - \frac{\lambda^2\widetilde{\omega}_0^2}{4\overline{\omega}_0^3}, \tag{15}$$

$x = a^\dagger + a$, $\alpha^2 = n_g$, and $\overline{\omega}_0(n_g)$ is shown in Eq. (11). The detailed derivation is presented in Appendix B. The ground state of $\widetilde{H}'_{\mathrm{sp}}$ is $|\psi_g^{\mathrm{sp}}\rangle = \mathcal{D}(\alpha)\mathcal{S}(r)|\tilde{\downarrow}, 0\rangle$, where $\mathcal{D}(\alpha) = \exp[\alpha(a^\dagger - a)]$ and $\mathcal{S}(r) = \lim_{r \to \infty}\exp[\frac{r}{2}(a^2 - a^{\dagger 2})]$. Its ground state energy is equal to the mean-field energy in Eq. (10). In Fig. 1(a), we show that the second derivative of the ground state energy is discontinuous at the critical point in the limit of $\eta \to$ and $N \to \infty$, which means the QPT that occurs in the *XXZ* central spin model is a second-order phase transition like the JC model [20]. In Fig. 1(b), we present the agreement between the analytical expression and the numerical simulation of the ground state energy. It shows that Eq. (10) agrees well with the numerical result when $|\Delta|$ is small relative to $\omega$; however, as $\Delta$ gets close to $-\omega$, the agreement becomes worse. The main reason for this problem is that when $\Delta$ is close to $-\omega$, the number of bath spins required for the numerical simulation becomes larger, which places a high demand on the memory of the computer.

## IV. INFLUENCE OF LONGITUDINAL INTERACTION

In this section, we will discuss the influence of the longitudinal interaction $\Delta$ on the excitation number $n_g$. The excitation number can be regarded as an order parameter since it keeps zero in the normal phase and becomes nonzero in the
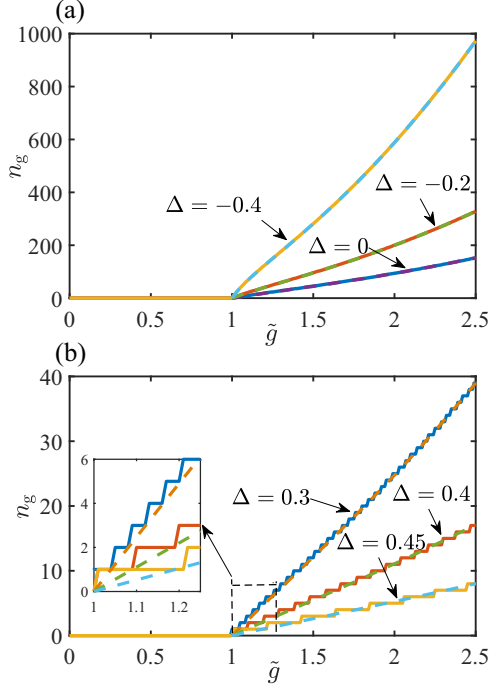
(a)

(b)

FIG. 2. Variations of the excitation number $n_g$ with respect to $\tilde{g}$. The solid lines are the numerical simulation and the dashed lines are the analytical expression given in Eq. (9). Here we set $\omega = 0.5$ and $\eta = 100$. In (a), the excitation numbers are significantly enhanced in the range of $-\omega < \Delta < 0$. The three lines from top to bottom correspond to $\Delta = -0.4, -0.2$, and $0$, respectively. In (b), the excitation numbers are suppressed in the range of $0 < \Delta < \omega$, and the curves become discontinued when $\Delta$ gets close to $\omega$. The three lines from top to bottom correspond to $\Delta = 0.3, 0.4$, and $0.45$, respectively.

superradiant phase. For $\Delta = 0$, $n_g$ can be described by Eq. (7); however, it is different for $-\omega < \Delta < 0$ and $0 < \Delta < \omega$, thus we must discuss it separately.

In Fig. 2(a), the analytical results given by Eq. (9) agree well with the numerical results for different negative longitudinal interaction. Moreover, we find a significant increase in the excitation number $n_g$ with an increasing absolute value of the longitudinal interaction $|\Delta|$ in the range of $-\omega < \Delta < 0$. We can explain this phenomenon in terms of the analytical expression Eq. (9), which can be rewritten as

$$n_g = \frac{\lambda^2(\lambda^2 + 2\Delta\widetilde{\omega}_0) - (\omega^2 - \Delta^2)\widetilde{\omega}_0^2}{2(\omega^2 - \Delta^2)(\lambda^2 + \Delta\widetilde{\omega}_0) + 2\lambda\omega\sqrt{(\omega^2 - \Delta^2)(\lambda^2 + 2\Delta\widetilde{\omega}_0)}}, \quad (16)$$

and we can find that Eq. (16) becomes Eq. (7) under the condition of $\Delta = 0$. It is easy to see that the numerator remains finite when $\Delta \simeq -\omega$, while the denominator tends to zero. Therefore, compared with the situation of $\Delta = 0$, the bath spins will be excited more quickly as $|\Delta|$ approaches to $\omega$.

But for $0 < \Delta < \omega$, the corresponding results are different. Figure 2(b) shows that the excitation number decreases as $\Delta$ increases, and when $\Delta$ is close enough to $\omega$, the variation of the excitation number $n_g$ with respect to $\tilde{g}$ becomes discontinuous (shape of a stair). Similarly, we seek an explanation from
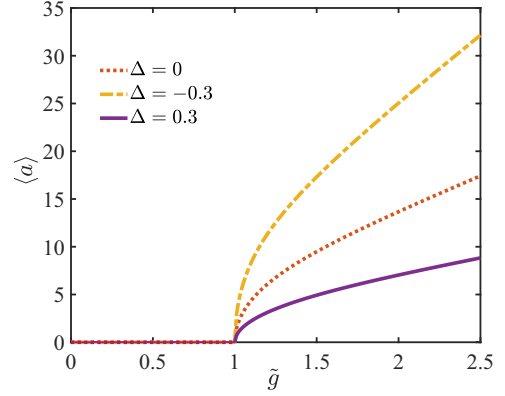


FIG. 3. Coherence of the ground state varies with $\tilde{g}$. For $-\omega < \Delta < 0$, the coherence increases significantly (yellow dot-dashed line), whereas for $0 < \Delta < \omega$, the coherence decreases appreciably (purple solid line).

Eq. (9). In the limit $\widetilde{\omega} = \omega - \Delta \to 0$, Eq. (9) becomes

$$n_g = \frac{\widetilde{\omega}_0}{2\Delta^2}(\tilde{g}\omega - \Delta). \quad (17)$$

In Eq. (17), for fixed $\tilde{g}$, the numerator decreases ($\tilde{g} > 1$ and $\tilde{g}\omega > \Delta$) and the denominator increases with an increase in $\Delta$, thus $n_g$ decreases. Besides, the excitation number $n_g$ is insensitive to $\tilde{g}$ when $\Delta$ is close to $\omega$, therefore $n_g$ will vary discretely [shown in Fig. 2(b)]. In summary, we see that the macroscopic excitations of bath spins are significantly enhanced in the case of the negative longitudinal interaction ($-\omega < \Delta < 0$), but for the situation of the positive longitudinal interaction ($0 < \Delta < \omega$), the excitations are suppressed.

Moreover, for the superradiant phase, the ground state coherence of bath spins in the limit of $\eta \to \infty$, $N \to \infty$ is given by

$$\langle a \rangle = \langle \psi_g^{\text{sp}} | a | \psi_g^{\text{sp}} \rangle = \sqrt{n_g}. \quad (18)$$

Similar to the excitation number of the ground state $n_g$, the coherence is also affected by the longitudinal interaction $\Delta$, which is shown in Fig. 3. In Fig. 3, we see that the results are similar to those of the excitation number discussed earlier. Furthermore, the coherence $\langle a \rangle$ is also an order parameter of the QPT, which can be viewed as the result of the $U(1)$ symmetry breaking [20].

## V. FINITE-SIZE EFFECT

To understand the *XXZ* central spin model more deeply, we need to consider the effect of a finite number of bath spins on this model. To end this, we use the mean-field approximation, and the excitation number of the ground state becomes

$$n_{g,\text{fs}} = -\frac{\lambda^2 + \Delta\widetilde{\omega}_0}{2\Lambda}$$
$$+ \frac{1}{2\Lambda}\sqrt{\frac{\omega^2[\lambda^4 + 2\Delta\lambda^2\widetilde{\omega}_0 + (\Delta^2 - \Lambda)\widetilde{\omega}_0^2]}{\omega^2 - \Lambda}}, \quad (19)$$

where $\Lambda = \Delta^2 - \lambda^2/N$. And the ground state energy is

$$E_{g,\text{fs}}^{\text{MF}} = \omega(n_{g,\text{fs}} - j) - \tfrac{1}{2}\overline{\omega}_0^{\text{fs}}(n_{g,\text{fs}}). \quad (20)$$
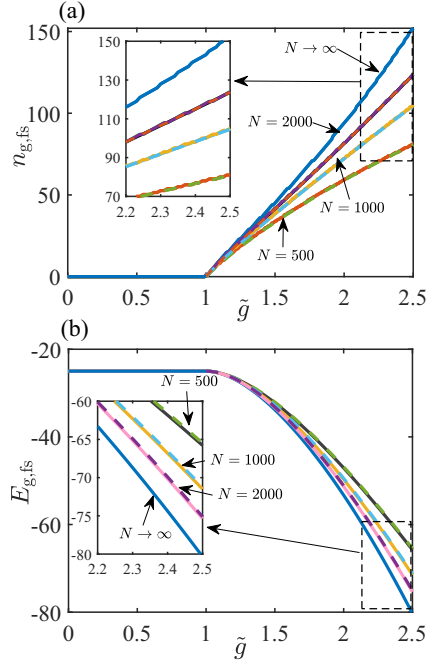
FIG. 4. Ground state excitation number and energy as a function of $\tilde{g}$ for the finite-size case. (a) The lines from top to bottom correspond to $N \to \infty$, $N = 2000$, $N = 1000$, and $N = 500$. The solid lines are the numerical simulation and the dashed lines are the analytical expression given in Eq. (19). (b) The lines from top to bottom correspond to $N = 500$, $N = 1000$, $N = 2000$, and $N \to \infty$. The dashed lines are the analytical expression given in Eq. (20).

More detailed derivations are presented in Appendix A. It is easy to verify that $\Lambda = \Delta^2$ and Eq. (19) becomes Eq. (9) in the limit of $N \to \infty$. In Fig. 4, we present the variation of the excitation number [shown in Fig. 4(a)] and the energy of the ground state [shown in Fig. 4(b)] with $\tilde{g}$. Note that the case where $N \to \infty$ in Fig. 4 corresponds to the analytical results given by Eqs. (9) and (14). Here we neglect the constant term in the ground state energy. It can be clearly seen that both the excitation number and the energy get closer to the results given by Eqs. (9) and (14) as $N$ increases. Figure 4 also shows that the analytical results (dashed lines) obtained by mean-field approximation are in good agreement with the the numerical results (solid lines).

Furthermore, we find that the effect of finite size on the excitation number and energy becomes more obvious as the coupling strength $\tilde{g}$ increases (shown in the subplots). This is due to the fact that Eq. (A7) can be approximated only under the condition that $N$ is much larger than $n_g$; however, this approximation becomes worse when $n_g$ increases with the coupling strength $\tilde{g}$. Therefore, in addition to the frequency ratio $\eta$ tending to infinity, the number of bath spins tending to infinity is also a necessary condition for the superradiant QPT to occur in the central spin model.

## VI. PRACTICAL APPLICATION IN QUANTUM METROLOGY

In this section, we consider the application in quantum metrology with the *XXZ* central spin model. Quantum
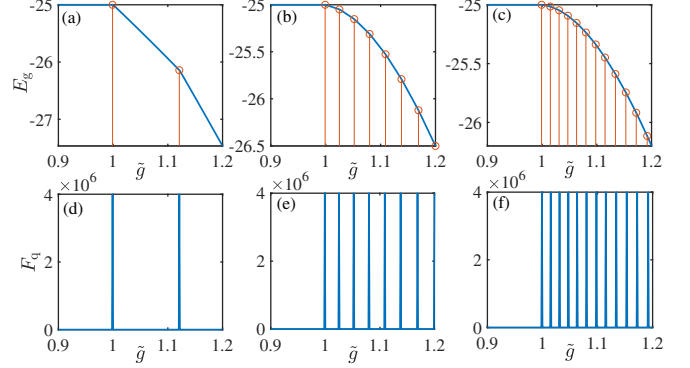


FIG. 5. Finite-frequency effect on the *XXZ* central spin model. (a)–(c) The level crossings for the ground state with $\eta = 10, 50, 100$. (d)–(f) The QFI $F_q$ as a function of $\tilde{g}$ with $\eta = 10, 50, 100$. As $\eta$ increases, the level crossings and the peaks of the QFI become increasingly dense.

criticality which can be viewed as a quantum resource has been widely applied to quantum metrology and quantum sensing [41,43,47–51]. Quantum Fisher information (QFI) is a key concept in quantum metrology, which gives the lower bound for the variance of the estimated parameter. In addition, the QFI proportional to fidelity susceptibility is used to quantify the abrupt change of the ground state in the vicinity of a critical point, and can be viewed as a good indicator for quantum phase transitions [42,52–54]. For a pure state $|\varphi(\tilde{g})\rangle$ with a parameter $\tilde{g}$, the QFI is given by

$$F_q = 4(\langle \partial_{\tilde{g}}\varphi(\tilde{g})|\partial_{\tilde{g}}\varphi(\tilde{g})\rangle - |\langle\varphi(\tilde{g})|\partial_{\tilde{g}}\varphi(\tilde{g})\rangle|^2). \quad (21)$$

Here we focus on the ground state of the *XXZ* central spin model. In the limit of $\eta \to \infty$ and $N \to \infty$, we have $|\varphi(\tilde{g})\rangle = |\psi_g^{np}\rangle = |\downarrow, 0\rangle$ for $\tilde{g} < 1$, and the QFI is $F_q = 0$. For $\tilde{g} > 1$, we have $|\varphi(\tilde{g})\rangle = |\psi_g^{sp}\rangle = \mathcal{D}(\alpha)\mathcal{S}(r)|\tilde{\downarrow}, 0\rangle$, and the QFI becomes

$$F_q = 4(\partial_{\tilde{g}}\alpha)^2 e^{2r} \to \infty, \quad (22)$$

where $\alpha = \sqrt{n_g}$ and $r \to \infty$. One can see that the QFI stays zero due to the invariant ground state in the normal phase, while in the superradiant phase, the QFI tends to infinity because of $r \to \infty$. In other words, the QFI changes drastically with the abrupt change of the system properties.

Now we discuss the finite-frequency effect on the QFI. In numerical simulation, we use the fidelity $f(\tilde{g}, \delta\tilde{g}) = |\langle\varphi(\tilde{g})|\varphi(\tilde{g} + \delta\tilde{g})\rangle|$ to calculate the QFI, which can be expressed as [54]

$$F_q = -4 \frac{\partial^2 f(\tilde{g}, \delta\tilde{g})}{\partial(\delta\tilde{g})^2}\bigg|_{\delta\tilde{g} \to 0}, \quad (23)$$

where $\delta g$ is a small perturbation. We set $\delta g = 10^{-3}$ in this paper. In Figs. 5(a)–5(c), we present the variation of the ground state energy and the level crossings between adjacent ground states $|\psi_-(n)\rangle$ and $|\psi_-(n+1)\rangle$ for different values of $\eta = 10, 50, 100$. As $\eta$ increases, the level crossings become denser. In Figs. 5(d)–5(f), we can see that the peaks of the QFI appear at the cross points of energy levels and also become denser with increasing $\eta$. Note that we have $F_q = 4 \times 10^6$ in Figs. 5(d)–5(f), which is due to the fact that Eq. (23) can be
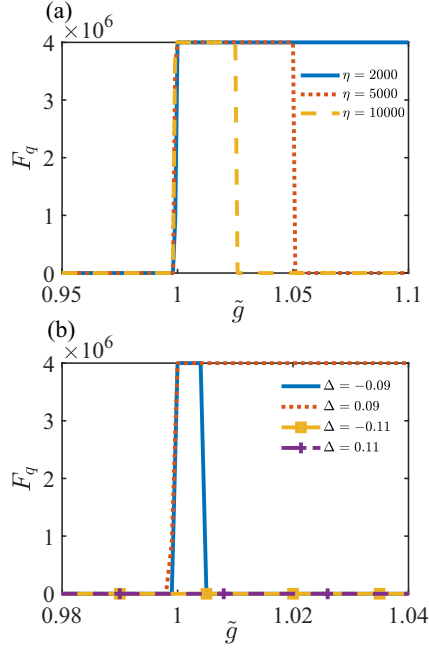
FIG. 6. (a) QFI for different frequency ratios $\eta$. The width of the QFI becomes narrower as $\eta$ increases. (b) QFI for different values of the longitudinal interaction $\Delta$. Here we set $\omega = 0.1$, $\eta = 10^4$, $N = 500$, and $\delta\tilde{g} = 10^{-3}$. The lines from top to bottom are $\Delta = -0.09$, 0.09, $-0.11$, and 0.11, respectively. There exist abrupt changes of the QFI for $|\Delta| < \omega$ ($|\Delta| = 0.09$); however, for $|\Delta| > \omega$ ($|\Delta| = 0.11$), these abrupt changes disappear.

written as [54]

$$F_q = \frac{4[1 - f(\tilde{g}, \delta\tilde{g})^2]}{(\delta\tilde{g})^2}, \tag{24}$$

and the fidelity is $f(\tilde{g}, \delta\tilde{g}) = 0$ at the cross points, thus we obtain $F_q = 4/(\delta g)^2$. In other words, the value of the QFI depends on the precision of $\delta\tilde{g}$, and in fact its value is divergent in the superradiant phase.

Moreover, the finite-frequency scaling behavior of the *XXZ* central spin model is quite different from that of the quantum Rabi model, which also undergoes a normal-superradiant phase transition in the limit of $\eta \to \infty$ [19]. In the quantum Rabi model, the finite-frequency scaling of the QFI around the critical point is [53]

$$F_q \sim \eta^\mu, \tag{25}$$

where $\mu = 4/3$. However, as shown in Fig. 5, the QFI of the *XXZ* central spin model at the critical point is divergent due to the level crossing between the ground state and the first excited state.

We also present the influence of finite size on the QFI in Fig. 6(a). We choose a relatively large frequency ratio ($\eta = 2000, 5000, 10\,000$) here, while the number of bath spins is relatively finite ($N = 500$), thus the ground state will not change when the excitation number $n_g$ reaches $N$. In Fig. 6(a), we can see that the QFI has an abrupt change at the critical point $\tilde{g}_c = 1$, and the width of the QFI becomes narrower as the frequency ratio $\eta$ increases. This phenomenon also requires that the number of bath spins $N \to \infty$ when the
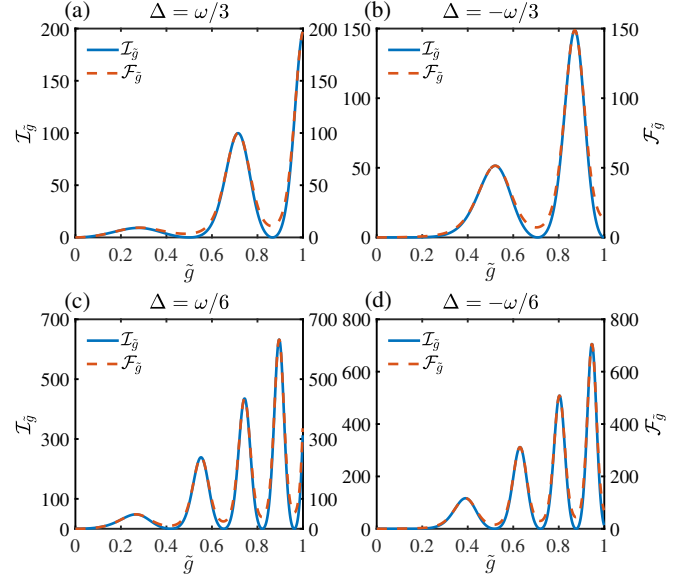


FIG. 7. Inverted variance $\mathcal{I}_{\tilde{g}}$ and the local quantum Fisher information $\mathcal{F}_{\tilde{g}}$ as functions of $\tilde{g}$ with different $\Delta$. In (a) and (b), we take the evolution time as $t = 2\pi/\tilde{\omega}$, and different values of $\Delta$ change the positions of the peaks. As the coupling strength approaches the critical point, the amplitude of oscillation increases. In (c) and (d), we take $t = 4\pi/\tilde{\omega}$, and the number of the peaks are nearly twice that of the previous one.

frequency ratio $\eta \to \infty$. Furthermore, we use the fidelity approach to verify the value range of the longitudinal interaction $\Delta$. In Fig. 6(b), we choose $\omega = 0.1$, $\eta = 10^4$, and find that the abrupt changes of the QFI disappear when $|\Delta| > \omega$.

In practical measurements, one can obtain the parameter information via suitable observables and the error propagation formula. In this model, the observable of the central spin $\langle\sigma_x\rangle$ is able to be measured. For $\tilde{g} < 1$, $\eta \to \infty$, and $N \to \infty$, it can be expressed as

$$\langle\sigma_x\rangle = \langle\psi_{\text{in}}|e^{iHt}\sigma_x e^{-iHt}|\psi_{\text{in}}\rangle$$
$$= 2\text{Re}\left\{b_\uparrow^* b_\downarrow \left\langle\varphi\left|e^{it[2\tilde{\omega}(\tilde{g}^2 + \frac{\Delta}{\omega})n]}\right|\varphi\right\rangle\right\}, \tag{26}$$

where $|\psi_{\text{in}}\rangle = (b_\uparrow|\uparrow\rangle + b_\downarrow|\downarrow\rangle) \otimes |\varphi\rangle$ and $|\varphi\rangle = \sum_n d_n|n\rangle$ with $\sum_n |d_n|^2 = 1$. The inverted variance of the parameter $\tilde{g}$ is given by [47,55]

$$\mathcal{I}_{\tilde{g}} = \frac{(\partial_{\tilde{g}}\langle\sigma_x\rangle)^2}{1 - \langle\sigma_x\rangle^2}. \tag{27}$$

We present the inverted variance $\mathcal{I}_{\tilde{g}}$ as a function of $\tilde{g}$ with different $\Delta$ in Fig. 7. The initial state we choose here is $b_\uparrow = b_\downarrow = 1/\sqrt{2}$, $|\varphi\rangle = |\alpha\rangle$ and $\alpha = 0.5$. In spin systems, the spin coherent state with a large number of bath spins can achieve the same effect and is feasible in practice [27,28].

To better compare these results, we calculate the local quantum Fisher information of the central spin, which is given by [55,56]

$$\mathcal{F}_{\tilde{g}} = \begin{cases} |\partial_{\tilde{g}}\boldsymbol{r}|^2 + \frac{(\boldsymbol{r}\cdot\partial_{\tilde{g}}\boldsymbol{r})}{1-|\boldsymbol{r}|^2}, & |\boldsymbol{r}| < 1, \\ |\partial_{\tilde{g}}\boldsymbol{r}|^2, & |\boldsymbol{r}| = 1, \end{cases} \tag{28}$$

where $\boldsymbol{r} = (\langle\sigma_x\rangle, \langle\sigma_x\rangle, \langle\sigma_x\rangle)$ is the Bloch vector. The first line of Eq. (28) corresponds to the mixed states and the second line corresponds to the pure states. The local quantum Fisher information gives the ultimate precision of the local measurement due to quantum Cramér-Rao bound, i.e.,

$$\Delta^2 \tilde{g} \geqslant \frac{1}{\mathcal{F}_{\tilde{g}}}, \tag{29}$$

where $\Delta^2 \tilde{g}$ is the variance of the parameter $\tilde{g}$. As shown in Fig 7, the inverted variance $\mathcal{I}_{\tilde{g}}$ (solid lines) and the local quantum Fisher information $\mathcal{F}_{\tilde{g}}$ (dashed lines) are almost equal for different $\Delta$ and evolution times $t$, especially at the maximum value. In other words, $\sigma_x$ can be regarded as the optimal observable that saturates the bound given by the local quantum Fisher information. Furthermore, it can be seen that $\mathcal{I}_{\tilde{g}}$ and $\mathcal{F}_{\tilde{g}}$ change periodically, and the amplitude of oscillation increases as the coupling strength $\tilde{g}$ approaches the critical point. It is worth noting that choosing different longitudinal interaction $\Delta$ has a significant influence on the positions of the maximum and minimum values of $\mathcal{I}_{\tilde{g}}$ and $\mathcal{F}_{\tilde{g}}$. It means that we can change the coupling strength $\tilde{g}$ at which maximum precision is achieved by controlling the value of the longitudinal interaction $\Delta$, instead of being confined to the vicinity of the critical point.

## VII. CONCLUSION

In this paper, we have investigated the quantum phase transition in the *XXZ* central spin model, and the exact energy spectrum can be given analytically due to the $U(1)$ symmetry. In addition, the similarity between the JC model and the central spin model is presented, and we have also demonstrated that the central spin model undergoes a superradiance QPT in the limit of $\eta \to \infty$ and $N \to \infty$. To further explain the QPT in this model, we utilize the mean-field approximation to obtain the mean-field energy and the excitation number, which agree well with the numerical simulation.

Moreover, the low-energy effective Hamiltonian given by the Schrieffer-Wolff transformation provides us with a new perspective to explain the quantum phase transition. Unlike the JC model, the nonlinear term caused by the longitudinal interaction can greatly affect the excitation number and the coherence of the ground state. For the case of $-\omega < \Delta < 0$, these two physical quantities increase significantly, while for the case of $0 < \Delta < \omega$ they decrease remarkably. We also consider the finite-size effect on the *XXZ* central spin model, and the analytical expression of the excitation number and energy of the ground state for different $N$ are given. Furthermore, we utilize the QFI to quantify the abrupt change of the ground state around the critical point, and propose a practical application scheme based on this model. This work reveals the superradiant QPT occurring in central spin systems and provides a new idea for the realization of criticality-enhanced quantum sensing.

## APPENDIX A: DERIVATION OF EXACT ENERGY SPECTRUM

Similar to the JC model, the dynamics of the *XXZ* central spin model is confined to the two-dimensional space spanned by $|\uparrow, n-1\rangle$ and $|\downarrow, n\rangle$ [45]. For a given $n$, the matrix elements of $H$ are

$$\langle\uparrow, n-1|H|\uparrow, n-1\rangle = \frac{\omega_0}{2} + (\omega + \Delta)m,$$

$$\langle\downarrow, n|H|\downarrow, n\rangle = -\frac{\omega_0}{2} + (\omega - \Delta)(m+1),$$

$$\langle\uparrow, n-1|H|\downarrow, n\rangle = \langle\downarrow, n-1|H|\uparrow, n\rangle = A\sqrt{k_n}, \tag{A1}$$

where $m = (n - 1 - j)$ and $k_n = (2j - n + 1)n$. The matrix representation is

$$H = \begin{pmatrix} \frac{\omega_0}{2} + (\omega + \Delta)m & A\sqrt{k_n} \\ A\sqrt{k_n} & -\frac{\omega_0}{2} + (\omega - \Delta)(m+1) \end{pmatrix}. \tag{A2}$$

We set $\Omega_1 = 2A\sqrt{k_n}$, $\Omega_2 = (2m+1)\Delta - \omega + \omega_0$, $\Omega_3 = \Delta - (2m+1)\omega$. Then we can obtain the energy eigenvalues given by

$$E_{\pm, n} = \frac{1}{2}\left(-\Omega_3 \pm \sqrt{\Omega_1^2 + \Omega_2^2}\right), \tag{A3}$$

and the eigenstates given by

$$|\psi_+(n)\rangle = \widetilde{P}_{\uparrow, n-1}^+ |\uparrow, n-1\rangle + \widetilde{P}_{\downarrow, n}^+ |\downarrow, n\rangle,$$

$$|\psi_-(n)\rangle = \widetilde{P}_{\uparrow, n-1}^- |\uparrow, n-1\rangle + \widetilde{P}_{\downarrow, n}^- |\downarrow, n\rangle, \tag{A4}$$

where

$$\widetilde{P}_{\uparrow, n-1}^\pm = \frac{\widetilde{\Omega} \pm \sqrt{1 + \widetilde{\Omega}^2}}{\sqrt{2(1 + \widetilde{\Omega}^2) \pm 2\widetilde{\Omega}\sqrt{1 + \widetilde{\Omega}^2}}},$$

$$\widetilde{P}_{\downarrow, n}^\pm = \frac{1}{\sqrt{2(1 + \widetilde{\Omega}^2) \pm 2\Omega\sqrt{1 + \widetilde{\Omega}^2}}}, \tag{A5}$$

and $\widetilde{\Omega} = \Omega_2/\Omega_1$. Now we use the mean-field approximation to get the mean-field energy. First, we apply the Holstein-Primakoff transformation to the Hamiltonian in Eq. (2), where the angular momentum operators are represented by

$$J_+ = \sqrt{N} a^\dagger \sqrt{1 - \frac{a^\dagger a}{N}}, \quad J_- = \sqrt{N} \sqrt{1 - \frac{a^\dagger a}{N}} a,$$

$$J_z = a^\dagger a - \frac{N}{2}. \tag{A6}$$

For large $N$, the Hamiltonian becomes

$$H_{\text{hp}} = \omega_0 S_z + \omega(a^\dagger a - j) + \lambda(a^\dagger S_- + a S_+)$$

$$+ 2\Delta\left(a^\dagger a - \frac{N}{2}\right)S_z, \tag{A7}$$

where $\lambda = A\sqrt{2j} = A\sqrt{N}$. The effective Hamiltonian under the mean-field approximation is given by

$$
\begin{aligned}
H_{\text{eff}} = \langle\beta|H_{\text{hp}}|\beta\rangle &= (\widetilde{\omega}_0 + 2\Delta|\beta|^2)S_z \\
&\quad + \omega(|\beta|^2 - j) + \lambda(\beta^*S_- + \beta S_+),
\end{aligned}
\tag{A8}
$$

and the mean-field energy is

$$
E^{\text{MF}}(|\beta|^2) = \omega(|\beta|^2 - j) - \tfrac{1}{2}\overline{\omega}_0,
\tag{A9}
$$

where $\overline{\omega}_0(|\beta|^2) = \sqrt{4\lambda^2|\beta|^2 + 4|\beta|^4\Delta^2 + 4|\beta|^2\Delta\widetilde{\omega}_0 + \widetilde{\omega}_0^2}$ is a function of $|\beta|^2$ and $\widetilde{\omega}_0 = \omega_0 - N\Delta$. Here we define $\tilde{g} = \lambda/\sqrt{\widetilde{\omega}\widetilde{\omega}_0}$ and replace $|\beta|^2$ with $n$. Utilizing $\partial E^{\text{MF}}/\partial n = 0$, we find that for $\tilde{g} < 1$ the excitation number of the ground state is still $n = n_g = 0$, and the mean-field energy is $E_g^{\text{MF}} = -\widetilde{\omega}_0/2 - \omega j$. However, for $\tilde{g} > 1$, we have

$$
n_g = -\frac{\lambda^2 + \Delta\widetilde{\omega}_0}{2\Delta^2} + \frac{\lambda\omega}{2\Delta^2}\sqrt{\frac{\lambda^2 + 2\Delta\widetilde{\omega}_0}{\omega^2 - \Delta^2}},
\tag{A10}
$$

and the energy of the ground state under the mean-field approximation is

$$
E_g^{\text{MF}} = (n_g - j)\omega - \tfrac{1}{2}\overline{\omega}_0(n_g).
\tag{A11}
$$

If we consider the finite-size effect, then utilizing Eqs. (A6) and (A8) we can obtain the following effective Hamiltonian:

$$
\begin{aligned}
H_{\text{eff}}^{\text{fs}} &= \omega_0 S_z + \omega(|\beta|^2 - j) + 2\Delta(|\beta|^2 - j)S_z \\
&\quad + \lambda\left(\beta^*\sqrt{1 - \frac{|\beta|^2}{N}}S_- + \beta\sqrt{1 - \frac{|\beta|^2}{N}}S_+\right),
\end{aligned}
\tag{A12}
$$

and the mean-field energy becomes

$$
E_{\text{fs}}^{\text{MF}} = \omega(n - j) - \tfrac{1}{2}\overline{\omega}_0^{\text{fs}},
\tag{A13}
$$

where $\overline{\omega}_0^{\text{fs}} = \sqrt{\widetilde{\omega}_0^2 + 4n^2\Lambda + 4\Delta n\widetilde{\omega}_0 + 4\lambda^2 n}$, and $\Lambda = \Delta^2 - \lambda^2/N$. Similarly, utilizing $\partial E_{\text{fs}}^{\text{MF}}/\partial n = 0$, we find the excitation number of the ground state for $\tilde{g} > 1$ is

$$
\begin{aligned}
n_{g,\text{fs}} = &-\frac{\lambda^2 + \Delta\widetilde{\omega}_0}{2\Lambda} \\
&+ \frac{1}{2\Lambda}\sqrt{\frac{\omega^2[\lambda^4 + 2\Delta\lambda^2\widetilde{\omega}_0 + (\Delta^2 - \Lambda)\widetilde{\omega}_0^2]}{\omega^2 - \Lambda}},
\end{aligned}
\tag{A14}
$$

and the ground state energy for the finite-size case is

$$
E_{g,\text{fs}}^{\text{MF}} = \omega(n_{g,\text{fs}} - j) - \tfrac{1}{2}\overline{\omega}_0(n_{g,\text{fs}}).
\tag{A15}
$$

## APPENDIX B: DERIVATION OF LOW-ENERGY EFFECTIVE HAMILTONIAN

In this section, we give the derivation of the low-energy effective Hamiltonian in Eq. (12). We first consider the case of the normal phase. $H_{\text{hp}}$ can be written as $H_{\text{hp}} = H_0 + V$, where

$$
\begin{aligned}
H_0 &= \widetilde{\omega}_0 S_z + \omega(a^\dagger a - j) + 2\Delta a^\dagger a S_z, \\
V &= \lambda(a^\dagger S_- + a S_+).
\end{aligned}
\tag{B1}
$$

Now we use the method proposed in Refs. [19,20]. First we apply a Schrieffer-Wolff transformation $e^S$ to $H_{\text{hp}}$, and the generator $S$ is anti-Hermitian and block-off-diagonal. Then the Hamiltonian becomes

$$
\widetilde{H} = e^{-S}H_{\text{hp}}e^S = \sum_{n=0}^{\infty}\frac{1}{n!}[H_{\text{hp}}, S]^{(n)},
\tag{B2}
$$

where $[H, S]^{(n)} = [[H, S]^{(n-1)}, S]$ and $[H, S]^{(0)} = H$. Here we need the block-off-diagonal part of $\widetilde{H}$ to be zero up to the second order in $\lambda$, thus $S$ must satisfy that

$$
[H_0, S] = -\lambda(a^\dagger S_- + a S_+).
\tag{B3}
$$

In the limit of $\eta \to \infty$, we find that when $S = \frac{\lambda}{\widetilde{\omega}_0}(a^\dagger S_- - a S_+)$, it leads to

$$
\begin{aligned}
\widetilde{H} &= H_0 + \frac{1}{2}[V, S] \\
&= H_0 + \frac{1}{2}\left[\lambda(a^\dagger S_- + a S_+), \frac{\lambda}{\widetilde{\omega}_0}(a^\dagger S_- - a S_+)\right] \\
&= H_0 + \frac{\lambda^2}{2\widetilde{\omega}_0}(4S_z a^\dagger a + 2S_z + \sigma_0),
\end{aligned}
\tag{B4}
$$

and the low-energy effective Hamiltonian is expressed as

$$
\begin{aligned}
\widetilde{H}_{\text{np}} &= \langle\downarrow|\widetilde{H}|\downarrow\rangle \\
&= -\frac{\widetilde{\omega}_0}{2} - \omega j + \widetilde{\omega}(1 - \tilde{g}^2)a^\dagger a,
\end{aligned}
\tag{B5}
$$

where $\widetilde{\omega} = \omega - \Delta$, $\tilde{g} = \lambda/\sqrt{\widetilde{\omega}\widetilde{\omega}_0}$.

For the superradiant phase, we need to apply a displacement operator $\mathcal{D}(\alpha)$ to $H_{\text{hp}}$, which is given by

$$
\begin{aligned}
\overline{H} &= \mathcal{D}^\dagger(\alpha)H_{\text{hp}}\mathcal{D}(\alpha) \\
&= \frac{\widetilde{\omega}_0}{2}\sigma_z + \omega a^\dagger a + \omega\alpha(a + a^\dagger) + \omega\alpha^2 + \lambda(a^\dagger\sigma_- + a\sigma_+) \\
&\quad + \lambda\alpha\sigma_x + \Delta[a^\dagger a + \alpha(a + a^\dagger) + \alpha^2]\sigma_z,
\end{aligned}
\tag{B6}
$$

where $\mathcal{D}(\alpha) = e^{\alpha(a^\dagger - a)}$, $\alpha^2 = n_g$, and here we make $\alpha$ to be real for convenience. Now we get rid of the superscript of the Pauli operators and denote $\sigma_i^{(0)} \equiv \sigma_i$ $(i = x, y, z)$ for convenience.

We find that the part of the central spin in Eq. (B6) is $(\widetilde{\omega}_0 + 2\Delta\alpha^2)\sigma_z/2 + \lambda\alpha\sigma_x$, and its eigenstates are

$$
|\tilde{\uparrow}\rangle = \cos\theta|\uparrow\rangle + \sin\theta|\downarrow\rangle, |\tilde{\downarrow}\rangle = -\sin\theta|\uparrow\rangle + \cos\theta|\downarrow\rangle,
\tag{B7}
$$

where $\theta = \frac{1}{2}\arctan(\frac{2\alpha\lambda}{2\alpha^2\Delta + \widetilde{\omega}_0})$. The corresponding eigenvalues are $\pm\frac{\overline{\omega}_0(\alpha^2)}{2} = \pm\frac{1}{2}\sqrt{4\lambda^2\alpha^2 + 4\alpha^4\Delta^2 + 4\alpha^2\Delta\widetilde{\omega}_0 + \widetilde{\omega}_0^2}$. Note that we have $\alpha^2 = n_g$, and utilizing Eq. (9) we have

$$
\begin{aligned}
\overline{\omega}_0(n_g) &= \sqrt{\frac{\lambda^4 + 2\Delta\lambda^2\widetilde{\omega}_0}{\omega^2 - \Delta^2}} \\
&= \tilde{g}\widetilde{\omega}_0\sqrt{\frac{\tilde{g}^2\widetilde{\omega} + 2\Delta}{\widetilde{\omega} + 2\Delta}}.
\end{aligned}
\tag{B8}
$$

Then we use the eigenstates $|\tilde{\uparrow}\rangle(|\tilde{\downarrow}\rangle)$ to rewrite Eq. (B6),

$$\overline{H} = \left(\frac{\lambda\widetilde{\omega}_0}{2\overline{\omega}_0}x - \frac{\lambda\Delta\alpha^2}{\overline{\omega}_0}x - \frac{2\Delta\alpha\lambda}{\overline{\omega}_0}a^\dagger a\right)\tau_x + \left(\frac{\overline{\omega}_0}{2} + \frac{\lambda^2\alpha}{\overline{\omega}_0}x + \frac{2\alpha^3\Delta^2 + \Delta\alpha\widetilde{\omega}_0}{\overline{\omega}_0}x + \frac{2\alpha^2\Delta^2 + \Delta\widetilde{\omega}_0}{\overline{\omega}_0}a^\dagger a\right)\tau_z$$
$$- \frac{\lambda}{2}p\tau_y + \omega\alpha^2 + \omega a^\dagger a + \omega\alpha x, \tag{B9}$$

where $x = a^\dagger + a$, $p = i(a^\dagger - a)$, and $\tau_{x,y,z}$ are the Paul operators in a new spin basis ($|\tilde{\uparrow}\rangle$, $|\tilde{\downarrow}\rangle$).

The Hamiltonian in Eq. (B9) can be divided into diagonal part $\overline{H}_0$ and off-diagonal part $\overline{V}$, where

$$\overline{H}_0 = \omega a^\dagger a + \omega\alpha x + \omega\alpha^2 - \omega j + \left(\frac{\overline{\omega}_0}{2} + \frac{\lambda^2\alpha}{\overline{\omega}_0}x + \frac{2\alpha^3\Delta^2 + \Delta\alpha\widetilde{\omega}_0}{\overline{\omega}_0}x + \frac{2\alpha^2\Delta^2 + \Delta\widetilde{\omega}_0}{\overline{\omega}_0}a^\dagger a\right)\tau_z,$$

$$\overline{V} = \left(\frac{\lambda\widetilde{\omega}_0}{2\overline{\omega}_0}x - \frac{\lambda\Delta\alpha^2}{\overline{\omega}_0}x - \frac{2\Delta\alpha\lambda}{\overline{\omega}_0}a^\dagger a\right)\tau_x - \frac{\lambda}{2}p\tau_y.$$

Then we need to find the generator $\overline{S}$ that satisfies $[\overline{H}_0, \overline{S}] = -\widetilde{V}$. In the $\eta \to \infty$ limit, $\overline{S}$ is given by

$$\overline{S} = \left(\frac{\lambda\widetilde{\omega}_0}{2i\overline{\omega}_0^2}x - \frac{\lambda\Delta\alpha^2}{i\overline{\omega}_0^2}x - \frac{2\Delta\alpha\lambda}{i\overline{\omega}_0^2}a^\dagger a\right)\tau_y + \frac{\lambda}{2i\overline{\omega}_0}p\tau_x. \tag{B10}$$

The transformed Hamiltonian is

$$\overline{H}' = \overline{H}_0 + \frac{1}{2}[\overline{V}, \overline{S}]$$

$$= \omega a^\dagger a + \omega\alpha x + \omega\alpha^2 - \omega j + \left(\frac{\overline{\omega}_0}{2} + \frac{\lambda^2\alpha}{\overline{\omega}_0}x + \frac{2\alpha^3\Delta^2 + \Delta\alpha\widetilde{\omega}_0}{\overline{\omega}_0}x + \frac{2\alpha^2\Delta^2 + \Delta\widetilde{\omega}_0}{\overline{\omega}_0}a^\dagger a\right)\tau_z$$

$$+ \left(\frac{\lambda^2\Delta^2\alpha^4}{\overline{\omega}_0^3} - \frac{\lambda^2\widetilde{\omega}_0\Delta\alpha^2}{\overline{\omega}_0^3} + \frac{\lambda^2\widetilde{\omega}_0^2}{4\overline{\omega}_0^3}\right)x^2\tau_z + \left(\frac{2\lambda^2\Delta^2\alpha^3}{\overline{\omega}_0^3} - \frac{\lambda^2\Delta\alpha\widetilde{\omega}_0}{\overline{\omega}_0^3}\right)(xa^\dagger a + a^\dagger ax)\tau_z$$

$$+ \frac{4\Delta^2\alpha^2\lambda^2}{\overline{\omega}_0^3}(a^\dagger a)^2\tau_z - \frac{\lambda^2\Delta\alpha^2}{\overline{\omega}_0^2} + \frac{\lambda^2\widetilde{\omega}_0}{2\overline{\omega}_0^2} - \frac{\lambda^2\Delta\alpha}{\overline{\omega}_0^2}x + \frac{\lambda^2}{4\overline{\omega}_0}p^2\tau_z. \tag{B11}$$

However, Eq. (B11) is too complicated to discuss further. By using numerical analysis, we find the terms with $\overline{\omega}_0^{-3}$ and $\overline{\omega}_0^{-2}$ except $\frac{\lambda^2\widetilde{\omega}_0^2}{4\overline{\omega}_0^3}x^2\tau_z$ are negligible, and finally we obtain the low-energy effective Hamiltonian

$$\overline{H}'_{\text{sp}} = \langle\tilde{\downarrow}|H'|\tilde{\downarrow}\rangle$$

$$= \omega\alpha^2 - \frac{\overline{\omega}_0}{2} + \kappa_0 x^2 + \kappa_1 x + \kappa_2 p^2 - \omega j, \tag{B12}$$

where

$$\kappa_0 = \frac{\omega}{4} - \frac{2\alpha^2\Delta^2 + \Delta\widetilde{\omega}_0}{4\overline{\omega}_0} - \frac{\lambda^2\widetilde{\omega}_0^2}{4\overline{\omega}_0^3}, \tag{B13}$$

$$\kappa_1 = \omega\alpha - \frac{\lambda^2\alpha + 2\alpha^3\Delta^2 + \Delta\alpha\widetilde{\omega}_0}{\overline{\omega}_0}, \tag{B14}$$

$$\kappa_2 = \frac{\omega}{4} - \frac{2\alpha^2\Delta^2 + \Delta\widetilde{\omega}_0 + \lambda^2}{4\overline{\omega}_0}. \tag{B15}$$

Utilizing Eqs. (9) and (B8), we find the relationship $2\Delta^2\alpha^2 + \lambda^2 + \Delta\widetilde{\omega}_0 = \omega\overline{\omega}_0$. It is easy to verify $\kappa_1 = \kappa_2 = 0$ with the above relationship. For $\Delta = 0$, Eq. (B13) becomes

$$\kappa_0 = \frac{\omega}{4}(1 - g^{-4}), \tag{B16}$$

which is consistent with the excitation energy $\epsilon_{\text{sp}}$ in the JC model [20]. Finally, we get Eq. (14) in the main text.

[1] S. Sachdev, *Quantum Phase Transitions*, 2nd ed. (Cambridge University Press, Cambridge, 2011).

[2] W. H. Zurek, U. Dorner, and P. Zoller, Dynamics of a Quantum Phase Transition, Phys. Rev. Lett. **95**, 105701 (2005).

[3] J. Dziarmaga, Dynamics of a Quantum Phase Transition: Exact Solution of the Quantum Ising Model, Phys. Rev. Lett. **95**, 245701 (2005).

[4] M. Heyl, A. Polkovnikov, and S. Kehrein, Dynamical Quantum Phase Transitions in the Transverse-Field Ising Model, Phys. Rev. Lett. **110**, 135704 (2013).

[5] T. D. Kühner and H. Monien, Phases of the one-dimensional Bose-Hubbard model, Phys. Rev. B **58**, R14741 (1998).

[6] M. Greiner, O. Mandel, T. Esslinger, T. W. Hänsch, and I. Bloch, Quantum phase transition from a superfluid to a Mott insulator in a gas of ultracold atoms, Nature (London) **415**, 39 (2002).

[7] M. Vojta, Quantum phase transitions, Rep. Prog. Phys. **66**, 2069 (2003).

[8] S. L. Sondhi, S. M. Girvin, J. P. Carini, and D. Shahar, Continuous quantum phase transitions, Rev. Mod. Phys. **69**, 315 (1997).

[9] B. Capogrosso-Sansone, N. V. Prokof'ev, and B. V. Svistunov, Phase diagram and thermodynamics of the three-dimensional Bose-Hubbard model, Phys. Rev. B **75**, 134302 (2007).

[10] R. H. Dicke, Coherence in spontaneous radiation processes, Phys. Rev. **93**, 99 (1954).

[11] K. Hepp and E. H. Lieb, On the superradiant phase transition for molecules in a quantized radiation field: The Dicke maser model, Ann. Phys. **76**, 360 (1973).

[12] A. D. Greentree, C. Tahan, J. H. Cole, and L. C. L. Hollenberg, Quantum phase transitions of light, Nat. Phys. **2**, 856 (2006).

[13] M. Gross and S. Haroche, Superradiance: An essay on the theory of collective spontaneous emission, Phys. Rep. **93**, 301 (1982).

[14] Y. K. Wang and F. T. Hioe, Phase transition in the Dicke model of superradiance, Phys. Rev. A **7**, 831 (1973).

[15] M. Liu, S. Chesi, Z.-J. Ying, X. Chen, H.-G. Luo, and H.-Q. Lin, Universal Scaling and Critical Exponents of the Anisotropic Quantum Rabi Model, Phys. Rev. Lett. **119**, 220601 (2017).

[16] X.-Y. Chen, Y.-Y. Zhang, L. Fu, and H. Zheng, Generalized coherent-squeezed-state expansion for the super-radiant phase transition, Phys. Rev. A **101**, 033827 (2020).

[17] M.-L. Cai, Z.-D. Liu, W.-D. Zhao, Y.-K. Wu, Q.-X. Mei, Y. Jiang, L. He, X. Zhang, Z.-C. Zhou, and L.-M. Duan, Observation of a quantum phase transition in the quantum Rabi model with a single trapped ion, Nat. Commun. **12**, 1126 (2021).

[18] Y.-Y. Zhang, Z.-X. Hu, L. Fu, H.-G. Luo, H. Pu, and X.-F. Zhang, Quantum Phases in a Quantum Rabi Triangle, Phys. Rev. Lett. **127**, 063602 (2021).

[19] M.-J. Hwang, R. Puebla, and M. B. Plenio, Quantum Phase Transition and Universal Dynamics in the Rabi Model, Phys. Rev. Lett. **115**, 180404 (2015).

[20] M.-J. Hwang and M. B. Plenio, Quantum Phase Transition in the Finite Jaynes-Cummings Lattice Systems, Phys. Rev. Lett. **117**, 123602 (2016).

[21] M. Tavis and F. W. Cummings, Exact solution for an *n*-molecule—radiation-field Hamiltonian, Phys. Rev. **170**, 379 (1968).

[22] E. M. Kessler, S. Yelin, M. D. Lukin, J. I. Cirac, and G. Giedke, Optical Superradiance from Nuclear Spin Environment of Single-Photon Emitters, Phys. Rev. Lett. **104**, 143601 (2010).

[23] M. J. A. Schuetz, E. M. Kessler, J. I. Cirac, and G. Giedke, Superradiance-like electron transport through a quantum dot, Phys. Rev. B **86**, 085322 (2012).

[24] S. Chesi and W. A. Coish, Theory of box-model hyperfine couplings and transport signatures of long-range nuclear-spin coherence in a quantum-dot spin valve, Phys. Rev. B **91**, 245306 (2015).

[25] Y. Fang, Y.-D. Wang, R. Fazio, and S. Chesi, Superradiantlike dynamics of nuclear spins by nonadiabatic electron shuttling, Phys. Rev. B **103**, 155301 (2021).

[26] G. A. Álvarez, E. P. Danieli, P. R. Levstein, and H. M. Pastawski, Environmentally induced quantum dynamical phase transition in the spin swapping operation, J. Chem. Phys. **124**, 194507 (2006).

[27] S. Dooley, F. McCrossan, D. Harland, M. J. Everitt, and T. P. Spiller, Collapse and revival and cat states with an *n*-spin system, Phys. Rev. A **87**, 052323 (2013).

[28] W.-B. He, S. Chesi, H.-Q. Lin, and X.-W. Guan, Exact quantum dynamics of XXZ central spin problems, Phys. Rev. B **99**, 174308 (2019).

[29] R. I. Nepomechie and X.-W. Guan, The spin-s homogeneous central spin model: Exact spectrum and dynamics, J. Stat. Mech.: Theory Exp. (2018) 103104.

[30] A. V. Khaetskii, D. Loss, and L. Glazman, Electron Spin Decoherence in Quantum Dots due to Interaction with Nuclei, Phys. Rev. Lett. **88**, 186802 (2002).

[31] G. Chen, D. L. Bergman, and L. Balents, Semiclassical dynamics and long-time asymptotics of the central-spin problem in a quantum dot, Phys. Rev. B **76**, 045312 (2007).

[32] M. Bortz, S. Eggert, C. Schneider, R. Stübner, and J. Stolze, Dynamics and decoherence in the central spin model using exact methods, Phys. Rev. B **82**, 161308(R) (2010).

[33] M. Bortz and J. Stolze, Exact dynamics in the inhomogeneous central-spin model, Phys. Rev. B **76**, 014304 (2007).

[34] G.-Q. Liu, J. Xing, W.-L. Ma, P. Wang, C.-H. Li, H. C. Po, Y.-R. Zhang, H. Fan, R.-B. Liu, and X.-Y. Pan, Single-Shot Readout of a Nuclear Spin Weakly Coupled to a Nitrogen-Vacancy Center at Room Temperature, Phys. Rev. Lett. **118**, 150504 (2017).

[35] M. Ahmadi, D. Jennings, and T. Rudolph, Dynamics of a quantum reference frame undergoing selective measurements and coherent interactions, Phys. Rev. A **82**, 032320 (2010).

[36] O. Landon-Cardinal and R. MacKenzie, Decoherence of a quantum gyroscope, Phys. Rev. A **85**, 022333 (2012).

[37] D. Šafránek, M. Ahmadi, and I. Fuentes, Quantum parameter estimation with imperfect reference frames, New J. Phys. **17**, 033012 (2015).

[38] V. Giovannetti, S. Lloyd, and L. Maccone, Quantum Metrology, Phys. Rev. Lett. **96**, 010401 (2006).

[39] V. Giovannetti, S. Lloyd, and L. Maccone, Advances in quantum metrology, Nat. Photonics **5**, 222 (2011).

[40] I. Frérot and T. Roscilde, Quantum Critical Metrology, Phys. Rev. Lett. **121**, 020402 (2018).

[41] P. Zanardi, M. G. A. Paris, and L. Campos Venuti, Quantum criticality as a resource for quantum estimation, Phys. Rev. A **78**, 042105 (2008).

[42] W.-L. You, Y.-W. Li, and S.-J. Gu, Fidelity, dynamic structure factor, and susceptibility in critical phenomena, Phys. Rev. E **76**, 022101 (2007).

[43] C. Invernizzi, M. Korbman, L. C. Venuti, and M. G. A. Paris, Optimal quantum estimation in spin systems at criticality, Phys. Rev. A **78**, 042106 (2008).

[44] M. Bina, I. Amelio, and M. G. A. Paris, Dicke coupling by feasible local measurements at the superradiant quantum phase transition, Phys. Rev. E **93**, 052118 (2016).

[45] C. Gerry and P. Knight, *Introductory Quantum Optics* (Cambridge University Press, Cambridge, 2004).

[46] H.-P. Eckle and H. Johannesson, A generalization of the quantum Rabi model: Exact solution and spectral structure, J. Phys. A: Math. Theor. **50**, 294004 (2017).

[47] Y. Chu, S. Zhang, B. Yu, and J. Cai, Dynamic Framework for Criticality-Enhanced Quantum Sensing, Phys. Rev. Lett. **126**, 010502 (2021).

[48] L. Garbe, M. Bina, A. Keller, M. G. A. Paris, and S. Felicetti, Critical Quantum Metrology with a Finite-Component Quantum Phase Transition, Phys. Rev. Lett. **124**, 120504 (2020).

[49] M. Raghunandan, J. Wrachtrup, and H. Weimer, High-Density Quantum Sensing with Dissipative First Order Transitions, Phys. Rev. Lett. **120**, 150501 (2018).

[50] H. T. Quan, Z. Song, X. F. Liu, P. Zanardi, and C. P. Sun, Decay of Loschmidt Echo Enhanced by Quantum Criticality, Phys. Rev. Lett. **96**, 140604 (2006).

[51] Y.-H. Ma and C.-P. Sun, Quantum sensing of rotation velocity based on transverse field Ising model, Eur. Phys. J. D **71**, 249 (2017).

[52] A. F. Albuquerque, F. Alet, C. Sire, and S. Capponi, Quantum critical scaling of fidelity susceptibility, Phys. Rev. B **81**, 064418 (2010).

[53] B.-B. Wei and X.-C. Lv, Fidelity susceptibility in the quantum Rabi model, Phys. Rev. A **97**, 013845 (2018).

[54] S.-J. Gu, Fidelity approach to quantum phase transitions, Int. J. Mod. Phys. B **24**, 4371 (2010).

[55] W. Ding, Y. Liu, Z. Zheng, and S. Chen, Dynamic quantum-enhanced sensing without entanglement in central spin systems, Phys. Rev. A **106**, 012604 (2022).

[56] W. Zhong, Z. Sun, J. Ma, X. Wang, and F. Nori, Fisher information under decoherence in Bloch representation, Phys. Rev. A **87**, 022337 (2013).